A Hybrid Analytical-Machine Learning Approach for LEO Satellite Orbit Prediction

Jamil Haidar-Ahmad[1], Nadim Khairallah[2], and Zaher M. Kassas[1,2]
[1]Department of Electrical Engineering and Computer Science, University of California, Irvine, USA
[2]Department of Mechanical and Aerospace Engineering, University of California, Irvine, USA
Emails: jhaidara@uci.edu, khairaln@uci.edu, and zkassas@ieee.org

***Abstract*—A hybrid analytical-machine learning (ML) framework for improved low Earth orbit (LEO) satellite orbit prediction is developed. The framework assumes the following three stages. (i) LEO satellite first pass: A terrestrial receiver with knowledge of its position produces carrier phase measurements from received LEO satellite signals, enabling it to estimate the time of arrival. The LEO satellite's states are initialized with simplified general perturbations 4 (SGP4)-propagated two-line element (TLE) data, and are subsequently estimated via an extended Kalman filter (EKF) during the period of satellite visibility. (ii) LEO satellite not in view: a nonlinear autoregressive with exogenous inputs (NARX) neural network is trained on the estimated ephemeris and is used to propagate the LEO satellite orbit for the period where the satellite is not in view. (iii) LEO satellite second pass: a terrestrial receiver with *no* knowledge of its position uses the ML-predicted LEO ephemeris along with its carrier phase measurements from received LEO signals to estimate its own position via an EKF. Experimental results with with signals from an Orbcomm satellite are presented to demonstrate the efficacy of the proposed framework. It is shown that during the satellite's second pass, the ML-predicted ephemeris error is reduced by nearly 90% from that of an SGP4 propagation. In addition, it is shown that if the receiver was to use the SGP4-predicted satellite ephemeris to localize itself, the EKF's initial position error of 2.2 km increases to 6.7 km, while the proposed framework reduces the position error to 448 m.**

***Keywords*—LEO satellites, machine learning, orbit determination, satellite tracking, signals of opportunity.**

I. Introduction

Future low Earth orbit (LEO) satellite constellations will weave a virtual blanket cover around the globe, bringing forth signals diverse in frequency and direction, which are also received at much higher power than global navigation satellite system (GNSS) signals [1], [2]. As such, LEO satellites are considered highly attractive from a positioning, navigation, and timing (PNT) perspective. LEO satellites' signals of opportunity could complement and safeguard GNSS to provide high levels of performance and operational resilience [3]–[5].

To exploit LEO satellites signals opportunistically, one must overcome three main challenges: (i) develop specialized receivers to extract navigation observables from these signals; (ii) estimate the satellites' clocks, which, unlike GNSS, are neither transmitted publicly nor are as stable and as tightly synchronized; and (iii) estimate the satellite's ephemeris with minimal error. The first two challenges have been the subject of extensive research recently [5]–[15]. This paper focuses on addressing the third challenge.

Several analytical and numerical satellite orbit determination algorithms have been developed to propagate satellites' states as well as associated uncertainty [16]. These propagators take into consideration, to various extents, multiple sources of perturbing forces, e.g., Earth's non-uniform gravitational field, atmospheric drag, solar radiation pressure, and third-body attraction (eg., Sun and Moon) [17]. The simplified general perturbations 4 (SGP4) [18] analytical propagator is used to generate ephemerides from a set of mean orbital elements given at a reference epoch in two-line elements (TLE) files, which are published and updated periodically by the North American Aerospace Defense Command (NORAD) [19]. However, analytical orbit determination methods are based on limited dynamical models and mean elements which may not meet PNT accuracy requirements [20], [21]. Space agencies usually employ high-precision orbit propagators (HPOP), which are numerical propagators used in conjunction with precise force models. However, numerical propagators require large amounts of data and significant computation time, which renders them undesirable for real-time PNT purposes.

Machine learning (ML) has shown tremendous potential in radar and communications [22], and its powerful modeling capabilities have been recently studied to provide a less parameter-reliant orbit propagation solution [23], [24]. In [25], [26], distribution regression was used for orbit determination of objects in LEO. Propagating LEO satellite orbits was studied in [27], [28] via artificial neural networks (ANNs), support vector machines (SVMs), and Gaussian processes (GPs). A simulation study developed in [28], [29] showed that ANNs possess high regression capabilities compared to SVMs and GPs. Several neural network (NN) architectures, such as the Time Delayed Neural Network (TDNN) and Long Short-Term Memory (LSTM) NNs were studied in [30]. However, utilizing ML in full orbit determination, allowing for completely replacing standard propagators, is yet to be achieved. Promising preliminary result were presented in [31], in which a TDNN was trained using the data from two Orbcomm LEO satellites, which broadcast their three-dimensional (3-D) position in the Earth-centered, Earth-fixed (ECEF) coordinate frame from onboard GNSS receivers. Finally, [32] utilized HPOP along with decoded Orbcomm satellite ephemeris messages to train a NN that was capable of estimating the position of the satellite to meter-level accuracy in a short time period.

This paper proposes a hybrid analytical-ML approach for LEO satellite orbit prediction where the receiver has no prior knowledge on the satellite's position except for publicly available TLE files. The paper makes the following contributions:

- A hybrid analytical-ML propagator is developed in a three-step framework: (i) refine LEO satellite's ephemeris via opportunistic tracking, initialized from an SGP4-propagated TLE, using an extended Kalman filter (EKF), (ii) train the ML propagator on the refined ephemeris *without* relying on the true ephemeris as was the case in [31], [32], and (iii) localize a receiver opportunistically with the ML-propagated ephemeris.
- The ephemeris propagation performance of the hybrid analytical-ML framework is compared with that of standalone propagators using true decoded Orbcomm ephemeris data.
- Experimental results are presented to demonstrate the efficacy of the proposed framework with a first pass of an Orbcomm satellite during which the tracking to refine the ephemeris is performed and a second pass of the same satellite during which the opportunistic localization performance using ML-propagated ephemeris and SGP4-propagated ephemeris are compared.

The paper is organized as follows. Section II describes the measurement model. Section III details the proposed analytical-ML orbit prediction framework. Section IV presents experimental results. Section V gives concluding remarks.

II. Carrier Phase Measurement Model

This section describes the carrier phase measurement model, which is used to both track the LEO satellite during its first pass and to localize the receiver from LEO satellite signals during the second pass. A LEO receiver extracts continuous-time carrier phase measurements from LEO satellites' signals by integrating the Doppler measurement over time [33]. The carrier phase measurement (expressed in meters) made by the receiver on the LEO satellite at time-step k, which represents discrete-time instant $t_k = kT + t_0$ for an initial time t_0, can be modeled in discrete-time as [2]

$$\begin{aligned}\phi(k) = \left\|\boldsymbol{r}_{\mathrm{r}}(k) - \boldsymbol{r}_{\mathrm{leo}}(k')\right\|_2 + c\left[\delta t_r(k) - \delta t_{\mathrm{leo}}(k'_l)\right] + \lambda N \\ + c\delta t_{\mathrm{iono}}(k) + c\delta t_{\mathrm{tropo}}(k) + v(k), \quad k = 1, 2, \ldots \quad (1)\end{aligned}$$

where k' represents discrete-time at $t_{k'} = kT + t_0 - \delta t_{\mathrm{TOF}}$, with δt_{TOF} being the true time-of-flight of the signal from the LEO satellite to the receiver; c is the speed-of-light; $\boldsymbol{r}_r$ and $\boldsymbol{r}_{\mathrm{leo}}$ are the receiver's and LEO satellite's 3-D position vectors expressed in the same reference frame; δt_r and δt_{leo} are the receiver's and LEO satellite's clock biases, respectively; λ is the wavelength of the carrier signal transmitted by the LEO satellite; N is the carrier phase ambiguity of the LEO satellite carrier phase measurement; δt_{iono} and $\delta t_{\mathrm{tropo}}$ are the ionospheric and tropospheric delays, respectively; and v is the measurement noise, which is modeled as a zero-mean white Gaussian random sequence with variance σ^2_ϕ.

Assuming no cycle slip occurs when the receiver tracks the carrier phase (i.e., the carrier phase ambiguity remains constant), the difference between the receiver and LEO satellite clock biases and the carrier phase ambiguity are lumped into a single term $c\Delta\delta t(k)$, simplifying (1) as

$$\begin{aligned}z(k) \triangleq \phi(k) = \left\|\boldsymbol{r}_r(k) - \boldsymbol{r}_{\mathrm{leo}}(k')\right\|_2 + c\Delta\delta t(k) \\ + c\delta t_{\mathrm{tropo}}(k) + c\delta t_{\mathrm{iono}}(k) + v(k), \quad (2)\end{aligned}$$

$$c\Delta\delta t(k) \triangleq c\left[\delta t_r(k) - \delta t_{\mathrm{sv}}(k')\right] + \lambda N. \quad (3)$$

III. Orbit Prediction Framework

PNT with measurements from overhead satellites require knowledge of the satellites' ephemeris. The best estimate available publicly for a LEO satellite's ephemeris would be from an initial ephemeris at a given time provided by TLE files published by NORAD, which would then be propagated through a propagator (e.g., SGP4). However, this initial ephemeris could be off by a few kilometers, and with SGP4 propagating the satellite's ephemeris through time, the error would continue to increase, only to be corrected when a new TLE file is published the next day. This limits the use of LEO signals for PNT, since such large ephemerides errors translate to unacceptably large positioning errors. The proposed framework mitigates the issue of relying on an ephemeris that is off by several kilometers. A base station with known position opportunistically tracks and refines the satellite's ephemeris when it is overhead. Next, an NN trains on this refined ephemeris and predicts the satellite's future position and velocity. Finally, a receiver with unknown position is given this predicted ephemeris to use it to localize itself when the same satellite passes overhead. Fig. 1 summarizes the proposed framework. The following subsections describe each stage of the proposed framework.

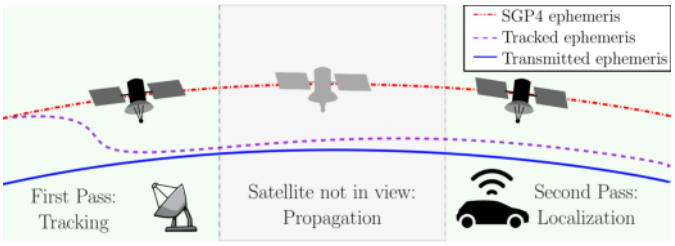

Fig. 1. Proposed framework. (i) LEO satellite first pass: A terrestrial receiver with knowledge of its position tracks the LEO satellite. The LEO satellite's states are initialized with SGP4-propagated TLE data, and are subsequently estimated via an EKF during the period of satellite visibility, utilizing the carrier phase measurements. (ii) LEO satellite not in view: an NN is trained on the estimated ephemeris and is used to propagate the LEO satellite orbit for the period where the satellite is not in view. (iii) LEO satellite second pass: a terrestrial receiver with *no* knowledge of its position uses the ML-predicted LEO ephemeris along with its carrier phase measurements from received LEO signals to estimate its own position via an EKF.

A. Opportunistic Tracking

This subsection formulates the EKF utilized as the tracking filter used to estimate the LEO satellite's ephemeris during the first LEO satellite pass in the proposed framework. The filter assumes a base station with known position making carrier

phase measurements modeled in (1). The EKF state vector is given by

$$\boldsymbol{x}_{\text{leo}} \;=\; \left[\boldsymbol{r}_{\text{leo}}^{\mathsf{T}},\, \dot{\boldsymbol{r}}_{\text{leo}}^{\mathsf{T}},\, c\Delta\delta t,\, c\Delta\dot{\delta} t\right]^{\mathsf{T}}.$$

For the satellite's time update between measurements, a two-body model including the most significant non-zero mean perturbing acceleration, which corresponds to J_2 effects, is adopted as the LEO satellite orbit dynamics model in the Earth-centered inertial (ECI) reference frame. This model offers a trade-off between accurate open-loop state prediction, while maintaining a simple analytical Jacobian for estimation error covariance propagation [34], and is given as

$$\ddot{\boldsymbol{r}}_{\text{leo}} = \boldsymbol{a}_{\text{grav},J_2} + \tilde{\boldsymbol{w}}_{\text{leo}}, \qquad \boldsymbol{a}_{\text{grav},J_2} = \frac{dU_{J_2}}{d\boldsymbol{r}_{\text{leo}}}, \tag{4}$$

where $\boldsymbol{r}_{\text{leo}} \triangleq [x_{\text{leo}},\, y_{\text{leo}},\, z_{\text{leo}}]^{\mathsf{T}}$ is the 3-D position vector of the LEO satellite in the ECI frame, $\boldsymbol{a}_{\text{grav},J_2}$ is the acceleration due to Earth's non-uniform gravity including J_2 effects, U_{J_2} is the non-uniform gravity potential of Earth including J_2 effects at the satellite, and $\tilde{\boldsymbol{w}}_{\text{leo}}$ is a process noise vector with power spectral density $\tilde{\mathbf{Q}}_{\text{leo}}$, which attempts to capture the overall acceleration perturbations including the unmodeled non-uniformity of Earth's gravitational field, atmospheric drag, solar radiation pressure, third-body gravitational forces (e.g., gravity of the Sun and Moon), and general relativity [17].

The components of $\boldsymbol{a}_{\text{grav},J_2} = [\ddot{x}_{\text{grav}},\, \ddot{y}_{\text{grav}},\, \ddot{z}_{\text{grav}}]^{\mathsf{T}}$ are

$$\begin{aligned}
\ddot{x}_{\text{grav}} &= -\frac{\mu x_{\text{leo}}}{\|\boldsymbol{r}_{\text{leo}}\|^3}\left[1 + J_2\frac{3}{2}\left(\frac{R_E}{\|\boldsymbol{r}_{\text{leo}}\|}\right)^2\left(1 - 5\frac{z_{\text{leo}}^2}{\|\boldsymbol{r}_{\text{leo}}\|^2}\right)\right],\\
\ddot{y}_{\text{grav}} &= -\frac{\mu y_{\text{leo}}}{\|\boldsymbol{r}_{\text{leo}}\|^3}\left[1 + J_2\frac{3}{2}\left(\frac{R_E}{\|\boldsymbol{r}_{\text{leo}}\|}\right)^2\left(1 - 5\frac{z_{\text{leo}}^2}{\|\boldsymbol{r}_{\text{leo}}\|^2}\right)\right],\\
\ddot{z}_{\text{grav}} &= -\frac{\mu z_{\text{leo}}}{\|\boldsymbol{r}_{\text{leo}}\|^3}\left[1 + J_2\frac{3}{2}\left(\frac{R_E}{\|\boldsymbol{r}_{\text{leo}}\|}\right)^2\left(3 - 5\frac{z_{\text{leo}}^2}{\|\boldsymbol{r}_{\text{leo}}\|^2}\right)\right],
\end{aligned} \tag{5}$$

where μ is Earth's standard gravitational parameter and R_E is the mean radius of the Earth. The clock error dynamics are assumed to evolve according to the standard double integrator model, driven by process noise [2].

B. ML-Based Orbit Prediction

After refining the satellite's ephemeris, the proposed ML model discussed in the following subsections trains on this ephemeris and then propagates it in time for usage in PNT.

1) Data Preparation: After tracking a satellite's ephemeris, this ephemeris is pre-processed for use in training the ML model. First, the accuracy of the two-body with J_2 propagation model on a short period of time is utilized for smoothing the tracked ephemeris. The tracked ephemeris is propagated over the entire tracking period allowing for a smoother training dataset and more training data points. The features selected as input candidates for the NN are satellite's 3-D position $\{x, y, z\}$ and velocity $\{\dot{x}, \dot{y}, \dot{z}\}$. The coordinate reference frame chosen is the ECI frame since this eliminates the time-varying effect of Earth's rotation in the ECEF frame.

2) Architecture: Two NNs, depicted in Figs. 2 and 3, are studied. The TDNN is based on a feed-forward NN (FFNN), which simply propagates from input to output in one direction. The time delay aspect is the NN's outputs being fed back as delayed inputs. Predicting a satellite's ephemeris can be seen as a time series prediction problem. The NARX architecture has been shown to be highly capable of learning long-term dependencies [35] and predicting time series [36]–[38]. The NARX takes SGP4 propagated position states as inputs. It also has a feedback loop where its output, the estimated ephemeris state values, are fed back as additional input.

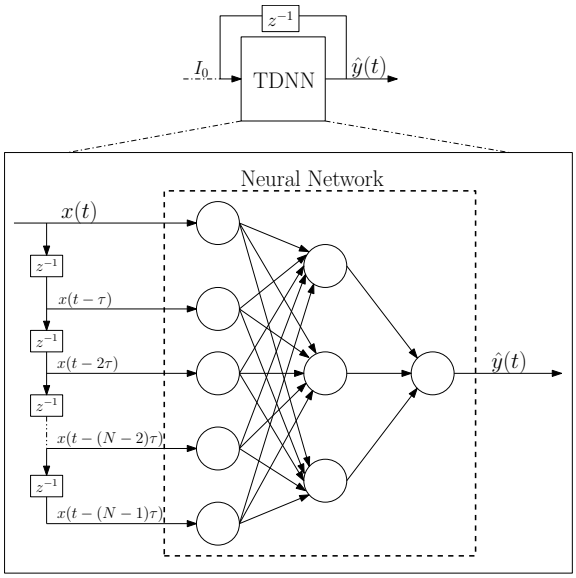

Fig. 2. TDNN Architecture.

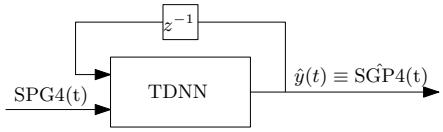

Fig. 3. NARX Architecture.

3) Optimization and Hyper-parameter Tuning: Next, hyper-parameters were chosen to best fit the learned model. Choosing the dimensions of the NN, such as how wide or how deep it is, will greatly affect its performance and ability to generalize, not memorize. Furthermore, since the dynamics of the error between SGP4 propagated ephemeris (initialized from a TLE file) and true satellite ephemeris are unknown and appear to be nonlinear, multiple activation functions must be investigated, including oscillatory functions (e.g., snake function). These hyper-parameters were carefully tuned, using a Bayesian optimization method, as well as compared with hyper-parameters selected by a HyperBand optimizer. Additionally, the number of time-delayed inputs was varied along with which states were fed into the NN. Finally, optimization was performed for incrementally decreasing the learning rate as training loss decreases, and early stopping was implemented to avoid over-fitting. Table I summarizes the search space the NNs were tuned on.

TABLE I
HYPER-PARAMETER SEARCH SPACE

Parameter	Value
Activation Function	Linear, ReLU, Tanh, Sigmoid, Snake [39]
Hidden Layers	[0,5]
Nodes per Layer	[2,128]
Optimizer	Adam [40], Adagrad [41], SGD, Yogi [42]

4) Results: After tuning the NN and comparing different possible combinations of hyper-parameters, it was concluded that a wide NN is capable of modeling SGP4-TLE ephemeris error, and any added layers in depth for introducing higher levels of abstraction are unnecessary. Moreover, increasing the number of delayed inputs degrades the performance as the dimensionality of the input increases without adding much information to the model. An important observation to note is that increasing the number of estimated states results in worse estimated ephemeris. This could be attributed to the limited size of data trained and validated on as well as the incrementally increasing levels of accuracy and abstraction required from the NN as more states are added. Finally, three NNs were trained, each estimating a position state and its time derivative. The NARX architecture given SGP4-ephemeris as exogenous inputs offered the best orbit propagation accuracy and therefore is chosen for the propagation step.

C. Localization

This subsection formulates the EKF used to estimate the receiver's position during the second LEO satellite pass in the proposed framework. The filter assumes a stationary receiver with unknown position and clocks. The receiver opportunistically extracts carrier phase measurements as modeled in (1). The EKF state vector is given by

$$\boldsymbol{x}_{\mathrm{r}} \;=\; \left[\boldsymbol{r}_{\mathrm{r}}^{\mathsf{T}},\, c\Delta\delta t_{\mathrm{r}},\, c\Delta\dot{\delta} t_{\mathrm{r}}\right]^{\mathsf{T}}.$$

IV. Experimental Results

This section demonstrates the proposed framework experimentally by (i) comparing the LEO tracking performance with a filter using the refined ML-propagated ephemeris versus using SGP4-propagated ephemeris initialized from TLE and (ii) localizing a stationary receiver with both ephemerides. An Orbcomm satellite was chosen, since it transmits the satellite's ephemeris. Signals from Orbcomm FM107 were collected, from which carrier phase measurements were opportunistically extracted. The satellite's downlink signals, which include the satellite's true ephemeris generated by on-board GPS receivers, were decoded for use as ground truth. Finally, ionospheric and tropospheric delays were corrected in the carrier phase measurements [43].

A. Experimental Setup

A very high frequency (VHF) quadrifilar helix antenna was connected to an Ettus E312 Universal Software Radio Peripheral (USRP) to sample Orbcomm LEO satellites' signals at 137-138 MHz at a sampling rate of 2.4 MSps. The USRP's oscillator was disciplined by an external, freely-running NI CDA-2990 OctoClock. The recording was repeated twice to record two consecutive passes of Orbcomm FM107 over Irvine, California, USA. The measurements extracted from the LEO satellite's signals during the first pass were used to track Orbcomm FM107 and refine its ephemeris. Then, this refined ephemeris was used as an input to the supervised training of the hybrid analytical-ML propagator. This propagator was subsequently employed to propagate the ephemeris of Orbcomm FM107 for around 100 minutes, which corresponds to its orbital period, until the satellite is visible again overhead. During the second pass, the measurements extracted from Orbcomm FM107 signals were used to opportunistically localize the receiver, while using the hybrid analytical-ML propagated ephemeris. The localization performance was compared to that obtained using the SGP4-propagated TLE ephemeris. The skyplot showing the trajectory of the satellite for both consecutive passes is shown in Fig. 4.

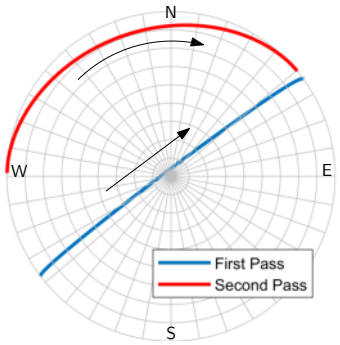

Fig. 4. Skyplot of satellite Orbcomm FM107 during the tracking (first pass) and localization (second pass).

B. Tracking

A receiver with known position tracks the LEO satellite according to the framework described in Section III-A. The state estimates are initialized according to

$$\hat{\boldsymbol{x}}_{\mathrm{leo}}(0|0) = [\boldsymbol{r}_{\mathrm{leo}}^{\mathsf{T}}(0), \dot{\boldsymbol{r}}_{\mathrm{leo}}^{\mathsf{T}}(0), \boldsymbol{z}(0) - \|\boldsymbol{r}_r - \boldsymbol{r}_{\mathrm{leo}}(0)\|_2\,, 0]^{\mathsf{T}},$$

where $[\boldsymbol{r}_{\mathrm{leo}}^{\mathsf{T}}(0), \dot{\boldsymbol{r}}_{\mathrm{leo}}^{\mathsf{T}}(0)]^{\mathsf{T}}$ is the satellite's initial state given from the SGP4-propagated ephemeris initialized from TLE. The initial estimation error covariance was set to

$$\begin{aligned}
&\mathbf{P}_{\boldsymbol{x}_{\mathrm{leo}}}(0|0) \triangleq \mathrm{diag}[\mathbf{P}_i(0|0), \mathbf{P}_{\mathrm{clk}}(0|0)]\\
&\mathbf{P}_i(0|0) \equiv {}^{i}_{b}\bar{\mathbf{R}}(0)\mathbf{P}_b(0|0)\,{}^{i}_{b}\bar{\mathbf{R}}^{\mathsf{T}}(0)\\
&{}^{i}_{b}\bar{\mathbf{R}}(0) = \mathrm{diag}[{}^{i}_{b}\mathbf{R}(0), {}^{i}_{b}\mathbf{R}(0)]\\
&\mathbf{P}_b(0|0) \equiv \mathrm{diag}[5\times10^5, 3\times10^3, 10^5, 0.05, 0.01, 0.2]\\
&\mathbf{P}_{\mathrm{clk}}(0|0) \equiv \mathrm{diag}[100, 10]
\end{aligned}$$

where $\mathbf{P}_i$ and $\mathbf{P}_b$ are the initial error covariance in the ECI frame and the satellite's body frame respectively, and ${}^{i}_{b}\mathbf{R}$ is the rotation matrix from the body frame to the ECI frame. This method initializes the estimate error covariance in the body frame which is more intuitive than initializing in the ECI frame, as most of the error is usually in the along-track. This

allows to capture the elliptical nature of the error covariance and initializes cross terms in the ECI frame which would allow for faster and better convergence. The measurement noise covariance was set to 0.5 m^2. The satellite was tracked for 517 seconds, during which, the satellite's position error magnitude decreased from 980 m to 56 m. Figs. 5 and 6 show the EKF error plots of the satellite's ephemeris in the body frame. The cross track direction is the least observable, which is consistent with [44]. Fig. 7 shows the position error magnitude of the tracked ephemeris compared to SGP4 propagated from TLE.

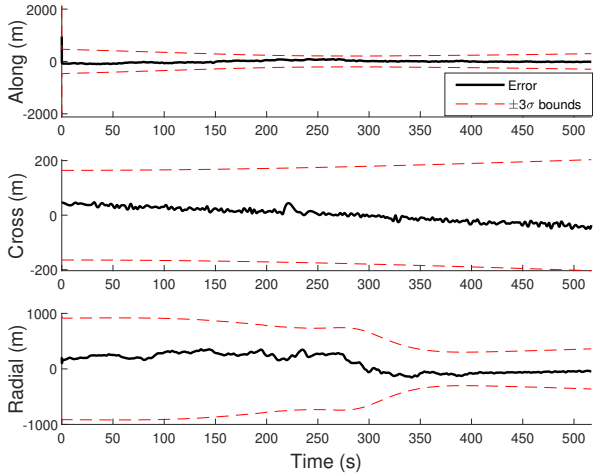

Fig. 5. EKF position plots in the satellite's body frame.

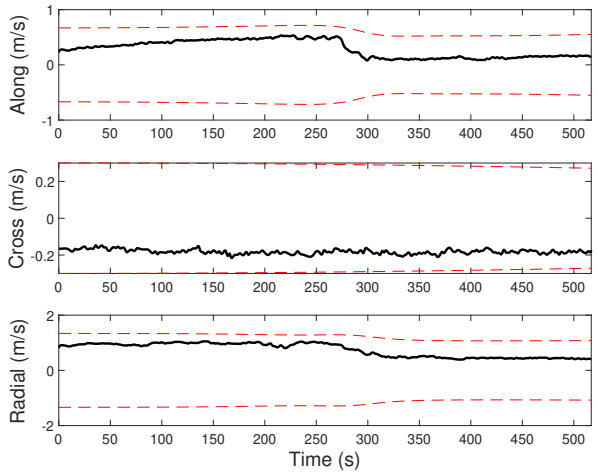

Fig. 6. EKF velocity plots in the satellite's body frame.

C. Propagation

Upon completion of satellite tracking, the estimated ephemeris at the final time of tracking is considered to be the best estimate for the satellite's ephemeris. This ephemeris is then back-propagated using the J_2 orbit propagation model to smooth over the tracking period. This smoothed ephemeris is now ready to be trained on. The ML model is given the SGP4 ephemeris propagated from TLE as exogenous input and the tracked and smoothed ephemeris as ground truth. The ML model then trains on this data and learns a mapping from the SGP4-TLE ephemeris to the tracked ephemeris. Finally, the ML model starts propagating and extrapolating satellite

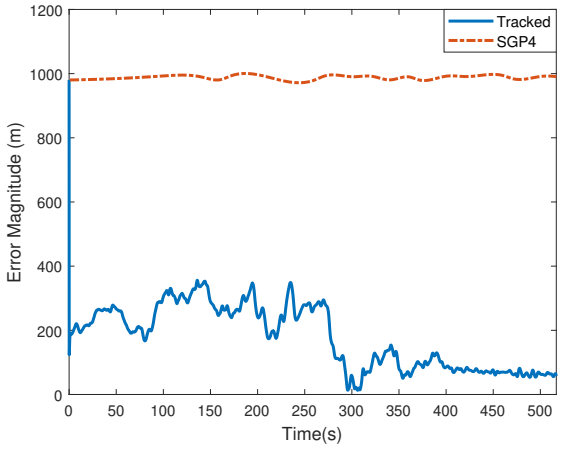

Fig. 7. Position error magnitude of SGP4 ephemeris initialized from TLE versus tracked ephemeris.

ephemeris, taking as its input the SGP4-TLE ephemeris at each time-step and its own outputs at previous time steps, and outputting a corrected ephemeris at that time-step. The ML model is propagated for 5,870 seconds until the satellite comes back to view. The ephemeris is then further propagated for a period of 363 seconds for this ephemeris to be used in localization. Fig. 8 shows the position error magnitude of the ML-propagated ephemeris and the SGP4-propagated ephemeris during the satellite's second pass.

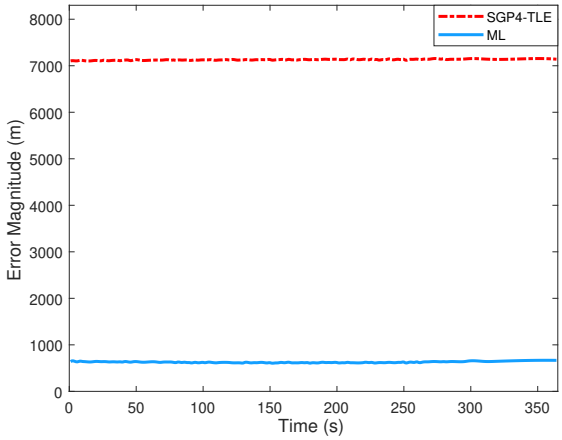

Fig. 8. Position error magnitude of SGP4 ephemeris initialized from TLE versus propagated ephemeris through the proposed ML framework.

D. Localization Results

The framework in Section III-C was adopted to localize a ground stationary receiver with the initial state estimates

$$\hat{\boldsymbol{x}}_r(0|0) = [\hat{\boldsymbol{r}}_r^{\mathsf{T}}(0|0), z(0) - \left\|\hat{\boldsymbol{r}}_r(0|0) - \boldsymbol{r}_{\text{leo}}^{j}(0)\right\|_2, 0]^{\mathsf{T}}$$

where $\hat{\boldsymbol{r}}_r(0|0)$ is the receiver's initial position estimate, which was drawn as $\hat{\boldsymbol{r}}_{\text{r}}(0|0) \sim \mathcal{N}[\boldsymbol{r}_r, \mathbf{P}_e(0|0)]$, in the ECEF frame. The estimate $c\Delta\delta t$ was initialized as the difference between the initial measurement and the estimated initial range, where

Fig. 9. Experimental results showing the initial and final 2-D stationary receiver localization errors and associated 95% uncertainty ellipses using (i) SGP4-propagated ephemeris and (ii) ML-propagated ephemeris. Map data: Google Earth.

$j \in \{\mathrm{ML}, \mathrm{SGP4}\}$ is the index of the satellite ephemeris used. The initial error covariance matrices were set as

$$\mathbf{P}_{\boldsymbol{x}_r}(0|0) \triangleq \mathrm{diag}[\mathbf{P}_e(0|0), \mathbf{P}_{\mathrm{clk}}(0|0)]$$
$$\mathbf{P}_e(0|0) \equiv {}^e_l\bar{\mathbf{R}}\mathbf{P}_l(0|0)\,{}^e_l\bar{\mathbf{R}}^{\mathsf{T}}$$
$$\mathbf{P}_l(0|0) \equiv \mathrm{diag}[10^6, 10^6, 0.1]$$
$$\mathbf{P}_{\mathrm{clk}}(0|0) \equiv \mathrm{diag}[10^8, 10^4]$$

where $\mathbf{P}_e(0|0)$ and $\mathbf{P}_l(0|0)$ are the initial receiver position error covariance in the ECEF frame and the local East-North-Up (ENU) frame, respectively, and ${}^e_l\mathbf{R}$ is the rotation matrix from the local ENU frame to the ECEF frame. This allows for comparing with the two-dimensional (2-D) North-East error only since the Up direction is poorly estimable from satellite measurements only. The measurement noise covariance was set to 0.5 m^2. The receiver was localized for 363 seconds, using the ML-propagated ephemeris as the satellite's ephemeris in the EKF filter. The 2-D magnitude of error decreased from an initial error of 2,219 m to 448 m. However, when the SGP4-propagated ephemeris was utilized with the same measurement noise covariance, the error increased to 6,718 m. Fig. 9 shows the the initial and final 2-D localization estimates and associated 95% uncertainty ellipses using (i) SGP4-propagated ephemeris and (ii) ML-propagated ephemeris. Fig. 10 shows the EKF error trajectories in the ENU frame.

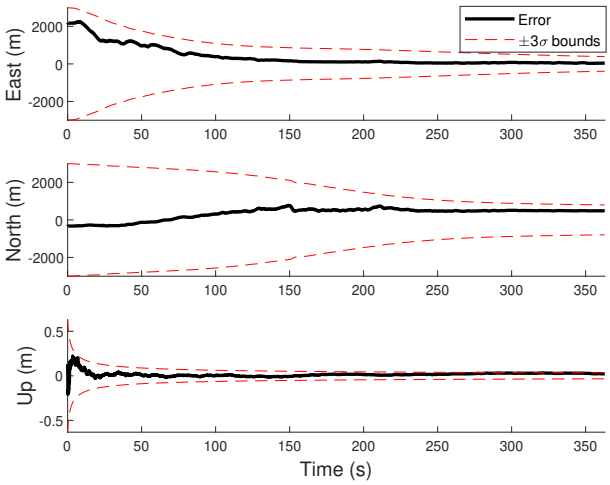

Fig. 10. EKF position plots for stationary localization using ML generated ephemeris.

V. Conclusion

This paper proposed a hybrid analytical-ML approach for LEO satellite orbit prediction, where the receiver has no prior knowledge on the satellite's position except for publicly available TLE files. During the LEO satellite's first pass, a stationary receiver tracks using carrier phase measurements the LEO satellite via an EKF initialized with SGP4-propagated TLE. A NARX NN is trained on the estimated ephemeris, which is then used to propagate the LEO ephemeris when the satellite is not in view. During the LEO satellite's second pass, a receiver with unknown position uses the ML-predicted LEO ephemeris to localize itself via an EKF. Experimental results with an Orbcomm LEO satellite are presented showing the efficacy of the proposed framework in reducing the initial receiver error from 2.22 km to 448 m, while the SGP4-ephemeris localization yielded a final error of 6.7 km.

Acknowledgments

This work was supported in part by the Office of Naval Research (ONR) under Grants N00014-19-1-2511 and N00014-19-1-2613, in part by the U.S. Department of Transportation (USDOT) under Grant 69A3552047138 for the CARMEN University Transportation Center (UTC), and in part by the Air Force Office of Scientific Research (AFOSR) under the Young Investigator Program award. The authors would like to thank Sharbel Kozhaya for his help with data collection and processing.

REFERENCES

[1] T. Reid, T. Walter, P. Enge, D. Lawrence, H. Cobb, G. Gutt, M. O'Conner, and D. Whelan, "Position, navigation, and timing technologies in the 21st century," J. Morton, F. van Diggelen, J. Spilker, Jr., and B. Parkinson, Eds. Wiley-IEEE, 2021, vol. 2, ch. 43: Navigation from low Earth orbit – Part 1: Concept, Current Capability, and Future Promise, pp. 1359–1379.

[2] Z. Kassas, "Position, navigation, and timing technologies in the 21st century," J. Morton, F. van Diggelen, J. Spilker, Jr., and B. Parkinson, Eds. Wiley-IEEE, 2021, vol. 2, ch. 43: Navigation from low Earth orbit – Part 2: models, implementation, and performance, pp. 1381–1412.

[3] T. Reid, B. Chan, A. Goel, K. Gunning, B. Manning, J. Martin, A. Neish, A. Perkins, and P. Tarantino, "Satellite navigation for the age of autonomy," in *Proceedings of IEEE/ION Position, Location and Navigation Symposium*, 2020, pp. 342–352.

[4] A. Nardin, F. Dovis, and J. Fraire, "Empowering the tracking performance of LEO'-based positioning by means of meta-signals," *IEEE Journal of Radio Frequency Identification*, pp. 1–1, 2021.

[5] Z. Kassas, M. Neinavaie, J. Khalife, N. Khairallah, J. Haidar-Ahmad, S. Kozhaya, and Z. Shadram, "Enter LEO on the GNSS stage: Navigation with Starlink satellites," *Inside GNSS Magazine*, vol. 16, no. 6, pp. 42–51, 2021.

[6] R. Landry, A. Nguyen, H. Rasaee, A. Amrhar, X. Fang, and H. Benzerrouk, "Iridium Next LEO satellites as an alternative PNT in GNSS denied environments–part 1," *Inside GNSS Magazine*, vol. 14, no. 3, pp. 56–64, May 2019.

[7] F. Farhangian and R. Landry, "Multi-constellation software-defined receiver for Doppler positioning with LEO satellites," *Sensors*, vol. 20, no. 20, pp. 5866–5883, October 2020.

[8] Z. Kassas, J. Morales, and J. Khalife, "New-age satellite-based navigation – STAN: simultaneous tracking and navigation with LEO satellite signals," *Inside GNSS Magazine*, vol. 14, no. 4, pp. 56–65, 2019.

[9] Q. Wei, X. Chen, and Y. Zhan, "Exploring implicit pilots for precise estimation of LEO satellite downlink Doppler frequency," *IEEE Communications Letters*, vol. 24, no. 10, pp. 2270–2274, 2020.

[10] T. Mortlock and Z. Kassas, "Performance analysis of simultaneous tracking and navigation with LEO satellites," in *Proceedings of ION GNSS Conference*, September 2020, pp. 2416–2429.

[11] F. Farhangian, H. Benzerrouk, and R. Landry, "Opportunistic in-flight INS alignment using LEO satellites and a rotatory IMU platform," *Aerospace*, vol. 8, no. 10, pp. 280–281, 2021.

[12] M. Neinavaie, J. Khalife, and Z. Kassas, "Acquisition, Doppler tracking, and positioning with Starlink LEO satellites: First results," *IEEE Transactions on Aerospace and Electronic Systems*, 2021, accepted.

[13] R. Cassel, D. Scherer, D. Wilburne, J. Hirschauer, and J. Burke, "Impact of improved oscillator stability on LEO-based satellite navigation," in *Proceedings of ION International Technical Meeting*, January 2022, pp. 893–905.

[14] C. Pinell, "Receiver architectures for positioning with low Earth orbit satellite signals," Master's thesis, Lulea University of Technology, School of Electrical Engineering, Sweden, 2021.

[15] N. Khairallah and Z. Kassas, "An interacting multiple model estimator of LEO satellite clocks for improved positioning," in *Proceedings of IEEE Vehicular Technology Conference*, 2022, accepted.

[16] B. Schutz, B. Tapley, and G. Born, *Statistical orbit determination*. Elsevier, 2004.

[17] J. Vetter, "Fifty years of orbit determination: Development of modern astrodynamics methods," *Johns Hopkins APL Technical Digest*, vol. 27, no. 3, pp. 239–252, November 2007.

[18] D. Vallado and P. Crawford, "SGP4 orbit determination," in *Proceedings of AIAA/AAS Astrodynamics Specialist Conference and Exhibit*, August 2008, pp. 6770–6799.

[19] North American Aerospace Defense Command (NORAD), "Two-line element sets," http://celestrak.com/NORAD/elements/.

[20] K. DeMars, R. Bishop, and M. Jah, "Entropy-based approach for uncertainty propagation of nonlinear dynamical systems," *Journal of Guidance, Control, and Dynamics*, vol. 36, no. 4, pp. 1047–1057, July-August 2013.

[21] X. Tian, G. Chen, E. Blasch, K. Pham, and Y. Bar-Shalom, "Comparison of three approximate kinematic models for space object tracking," in *Proceedings of International Conference on Information Fusion*, 2013, pp. 1005–1012.

[22] U. Majumder, E. Blasch, and D. Garren, *Deep Learning for Radar and Communications Automatic Target Recognition*. Norwood, MA: Artech House, 2020.

[23] Y. Wang, X. Bai, H. Peng, G. Chen, D. Shen, E. Blasch, and C. Sheaff, "Gaussian-binary classification for resident space object maneuver detection," *Acta Astronautica*, vol. 187, pp. 438–446, October 2021.

[24] S. Shen, C. Sheaff, M. Guo, E. Blasch, K. Pham, and G. Chen, "Three-dimensional convolutional neural network (3D-CNN) for satellite behavior discovery," in *Proceedings of SPIE Sensors and Systems for Space Applications*, vol. 11755, 2021, pp. 1–18.

[25] S. Sharma and J. Cutler, "Robust orbit determination and classification: A learning theoretic approach," *IPN Progress Report*, pp. 42–203, 2015.

[26] F. Feng, Y. Zhang, H. Li, Y. Fang, Q. Huang, and X. Tao, "A novel space-based orbit determination method based on distribution regression and its sparse solution," *IEEE Access*, vol. 7, pp. 133 203–133 217, 2019.

[27] H. Peng and X. Bai, "Limits of machine learning approach on improving orbit prediction accuracy using support vector machine," in *Proceedings of Advanced Maui Optical and Space Surveillance Technologies Conference*, 2017, pp. 1–22.

[28] H. Peng and X. Bai, "Artificial neural network–based machine learning approach to improve orbit prediction accuracy," *Journal of Spacecraft and Rockets*, vol. 55, no. 5, pp. 1248–1260, 2018.

[29] H. Peng and X. Bai, "Comparative evaluation of three machine learning algorithms on improving orbit prediction accuracy," *Astrodynamics*, vol. 3, no. 4, pp. 325–343, 2019.

[30] N. Salleh, S. Yuhaniz, N. Azmi, and S. Sabri, "Enhancing simplified general perturbations-4 model for orbit propagation using deep learning: a review," in *Proceedings of International Conference on Software and Computer Applications*, 2019, pp. 5937–5941.

[31] T. Mortlock and Z. Kassas, "Assessing machine learning for LEO satellite orbit determination in simultaneous tracking and navigation," in *Proceedings of IEEE Aerospace Conference*, March 2021, pp. 1–8.

[32] S. Kozhaya, J. Haidar-Ahmad, A. Abdallah, Z. Kassas, and S. Saab, "Comparison of neural network architectures for simultaneous tracking and navigation with LEO satellites," in *Proceedings of ION GNSS Conference*, September 2021, pp. 2507–2520.

[33] P. Misra and P. Enge, *Global Positioning System: Signals, Measurements, and Performance*, 2nd ed. Ganga-Jamuna Press, 2010.

[34] J. Morales, J. Khalife, U. Santa Cruz, and Z. Kassas, "Orbit modeling for simultaneous tracking and navigation using LEO satellite signals," in *Proceedings of ION GNSS Conference*, September 2019, pp. 2090–2099.

[35] T. Lin, B. Horne, P. Tino, and C. Giles, "Learning long-term dependencies in NARX recurrent neural networks," *IEEE Transactions on Neural Networks*, vol. 7, no. 6, pp. 1329–1338, 1996.

[36] H. Siegelmann, B. Horne, and C. Giles, "Computational capabilities of recurrent NARX neural networks," *IEEE Transactions on Systems, Man, and Cybernetics, Part B (Cybernetics)*, vol. 27, no. 2, pp. 208–215, 1997.

[37] H. Xie, H. Tang, and Y. Liao, "Time series prediction based on NARX neural networks: An advanced approach," in *Proceedings of IEEE International Conference on Machine Learning and Cybernetics*, vol. 3, 2009, pp. 1275–1279.

[38] J. Menezes, P. Maria, and G. Barreto, "Long-term time series prediction with the NARX network: An empirical evaluation," *Neurocomputing*, vol. 71, no. 16-18, pp. 3335–3343, 2008.

[39] L. Ziyin, T. Hartwig, and M. Ueda, "Neural networks fail to learn periodic functions and how to fix it," *Advances in Neural Information Processing Systems*, vol. 33, pp. 1583–1594, 2020.

[40] D. Kingma and J. Ba, "Adam: A method for stochastic optimization," *arXiv preprint arXiv:1412.6980*, 2014.

[41] J. Duchi, E. Hazan, and Y. Singer, "Adaptive subgradient methods for online learning and stochastic optimization," *Journal of Machine Learning Research*, vol. 12, no. 7, pp. 2121–2159, 2011.

[42] M. Zaheer, S. Reddi, D. Sachan, S. Kale, and S. Kumar, "Adaptive methods for nonconvex optimization," in *Proceedings of International Conference on Neural Information Processing Systems*, vol. 31, 2018, pp. 9815–9825.

[43] J. Khalife, M. Neinavaie, and Z. Kassas, "Navigation with differential carrier phase measurements from megaconstellation LEO satellites," in *Proceedings of IEEE/ION Position, Location, and Navigation Symposium*, April 2020, pp. 1393–1404.

[44] N. Khairallah and Z. Kassas, "Ephemeris closed-loop tracking of LEO satellites with pseudorange and Doppler measurements," in *Proceedings of ION GNSS Conference*, September 2021, pp. 2544–2555.